PULSED MAGNETIC NOZZLE
for Fusion Propulsion

JASON CASSIBRY, BRYAN WINTERLING AND KEVIN SCHILLO, Propulsion Research Center, University of Alabama in Huntsville, Huntsville, AL 35899 USA

email Jason.Cassibry@uah.edu

A fusion or pulsed fission/fusion hybrid propulsion system has the potential to enable rapid interplanetary, deep-space and interstellar precursor missions. For these systems, one of the problems to be solved is the design and development of a nozzle to convert isotropic thermal expansion of a burning target into directed thrust. This paper presents three dimensional simulations of magnetic nozzles to generate propulsive thrust from deuterium tritium plasma. Of interest, was the discovery of a novel winding of field coils, longitudinally rather than azimuthally, to help promote a higher component of jxB Lorentz force in the axial direction. Gravitational lensing and interstellar precursor missions were investigated using gravity free straight line trajectory analysis to determine notional performance requirements to assess the needed improvements in the approach and results presented in this study.

Keywords: Fusion propulsion, Fission/fusion hybrid propulsion, Magnetic nozzle

1 INTRODUCTION

A fission/fusion hybrid or pure fusion propulsion system offers a potential path to enabling rapid interplanetary travel. Using straight line trajectory mission analysis assuming continuous thrust for 2/3 of the trip distance (1/3 acceleration, 1/3 coast, 1/3 deceleration each way), round trip times for notional deep-space sample return missions using a vehicle with a specific power of 1 kw/kg are plotted in Fig. 1 for destinations from Jupiter out to the dwarf planet Eris. The travel time to and from Jupiter can be less than three years, while samples return from the dwarf planets out to Eris can be accomplished between 10 and 17 years. Studies conducted by Cassibry et al [1], Miernik et al [2] and Adams et al [3] have also shown that round trip, human piloted missions to Mars can be two to six months: thus, greatly reducing the need to wait for period launch windows. Although more demanding, interstellar precursor missions have also been considered and are summarized in an extensive report by Schulze [4], with flyby times ranging from ~50 years to a few centuries depending on assumptions about propulsion technology and destination.

A fusion propulsion system must have a mechanism to redirect an expanding fusion plasma in an axial direction in order to impart a propulsive momentum on the spacecraft. A simple option, explored during Project Orion in the 1950s and 60s, suggested a pusher plate at the rear of the spacecraft. Nuclear explosives were to be ejected and detonated at a certain distance from the spacecraft, with the plasma generated by the explosion then impacting the pusher plate and propelling the vehicle forward [5]. The primary momentum imparted is due to the stagnation and expansion of the propellant against this plate, however in an actual system, ablation of the pusher plate may contribute a non-negligible thrust component which would require experiments to quantify. A slight variant investigated by the authors of this paper involved replacing the pusher plate with a hemispherical nozzle, which was found to offer a higher specific impulse [6]. There have been some analytical models and engineering design of coils, such as in the Human Outer Planet Exploration (HOPE) study [3]. The most recent and rigorous work in this area was a 2D MHD simulation of a parabolic nozzle shape, building on the HOPE study [7]. These preliminary results suggest that plasma reflection and redirection can be achieved but instabilities at the vacuum/plasma boundary interface introduce difficulties which must

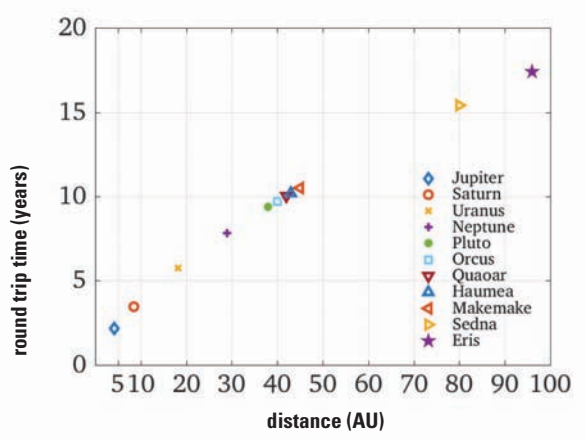

Fig.1 Comparison of roundtrip times for a 1 kW/kg fusion propulsion powered spacecraft to destinations spanning from Jupiter to Eris. The locations of the outer dwarf planets are estimated based on anticipated distance from a 2017 launch date from LEO.

This paper was presented at the Tennessee Valley Interstellar Workshop 2017 Symposium, Huntsville, USA.

be addressed. This paper presents numerical results for a 3D pulsed magnetic nozzle, which may offer an improved propulsion mechanism over a pusher plate or solid-state nozzle, with anticipated longer lifetimes since the plasma does not come in direct contact with the coils generating the nozzle. To the authors' knowledge this is the first such work in a 3D simulation.

2 NUMERICAL METHOD

All simulations are performed with the Smoothed Particle Fluid with Maxwell equation solver (SPFMax) [8]. Smoothed Particle Hydrodynamics (SPH) [9] is a meshless Lagrangian method that simulates hydrodynamics by dividing a fluid into a set of particles and using a summation interpolant function to calculate the properties and gradients for each of these particles. In simple terms, the SPH method is nothing more than an algorithm for interpolation of properties and gradients from scattered data in 1, 2, and 3 dimensions. There are two approximations that are made. First, the interpolation of a property of a field can be determined by the integral approximation

$$A_a(r) = \int A\,(r')W(r-r',h)dr' \tag{1}$$

where A is any property (like temperature, pressure, etc), subscript a means point or particle a, r is the position of point a in space, and W is the interpolating kernel function. In the limit that $h\to 0$, W becomes the direct delta function and the expression becomes exact. Any function can be approximated in this way, and this is the first assumption of SPH. The second assumption is to replace the integral with a summation,

$$A_a = \sum_b A_b\, V_b W_{ab}(r-r',h) \tag{2}$$

where V_b is the volume of the neighboring particles b. This is called the summation or particle approximation, and is analogous to discretizing a computational volume into a mesh for finite difference or finite element algorithms. The kernel function W is usually a Gaussian-like or cubic b-spline function which goes to zero at some κh, where κ=2 normally. Gradients can be approximated as

$$\nabla A_a = \sum_b A_b\, V_b \nabla W_{ab}(r-r',h) \tag{3}$$

In SPFMax, the cubic spline function is used,

$$W_{ab} = \begin{cases} \frac{1}{4\pi {h_{ab}}^3}[(2-q)^3 - 4(1-q)^3], & for \quad 0 \le q \le 1 \\ \frac{1}{4\pi {h_{ab}}^3}(2-q)^3, & for \quad 1 \le q \le 2 \\ 0 & for \quad q > 2 \end{cases} \tag{4}$$

where q is the ratio of the radius from particle a to the neighbor particle b to the particle h size. The key to implementing any SPH method properly is to have an accurate list of neighbors for each particle and a compact support distance h which scales the kernel function and its gradients so the following constraints are satisfied:

$$\sum_b V_b\, W_{ab} = 1 \tag{5}$$

and the first moment is:

$$\sum_b V_b\, \nabla W_{ab} = 0 \tag{6}$$

Higher order moments such as second order derivatives also sum to 0. The particle volume is:

$$V_a = \frac{h_a^3}{\eta^3} \tag{7}$$

and η is 1.11 in SPFMax, and variations on that value will require adjustments to h so that the constraints remain satisfied. Thus, the gradients in a fluid or plasma are calculated at a specific particle location using the particle volume and proximity of other nearby particles [10] [11]. For second order derivatives in SPFMax, the code stores first order derivatives as particle properties in which second order derivatives are needed [12], [13]. This includes the three spatial derivatives of each of the three velocity components [14, 15] as well as the scalar temperature for the heat conduction equation [16]. Details of the SPH method can be found in Ref. [9].

SPFMax solves conservation of mass exactly because the continuity equation is not necessary. Rather, density is determined by the particle mass divide by the particle volume, where the mass is a constant property of the particles. The momentum equation for a single fluid is given by:

$$\frac{\partial u}{\partial t} = -\frac{1}{\rho}\nabla \mathrm{p} + \nabla\cdot\tau + \frac{1}{\rho} j\times B \tag{8}$$

where p is the static pressure and τ is the deviatoric viscous stress tensor. The single temperature energy equation ($T_i = T_e = T$) is given by:

$$\frac{\partial e}{\partial t} = -\frac{p}{\rho}\nabla\cdot u + \frac{\tau}{\rho}\nabla\cdot u - \nabla\cdot(k\nabla T) - 4\sigma \mathrm{T}^4 \chi_{\mathrm{Planck}} + \frac{\eta}{\rho} j^2 \tag{9}$$

where k is the thermal conductivity, σ is the Stefan-Boltzmann constant, T is temperature and χ_{Planck} is the single group Planck emission opacity. Alternatively, if the optical thickness $1/(\rho\chi_{\mathrm{Planck}})$ is of the same order or smaller than the particle scale h, then radiation can be modeled as a diffusion process. This is achievable by adding an additional term to the overall thermal conductivity [17]:

$$k_{\mathrm{total}} = \mathrm{k} + \mathrm{k}_{\mathrm{Ross}} = \mathrm{k} + \frac{4\mathrm{acT}_e^3}{3\rho\chi_{\mathrm{Ross}}} \tag{10}$$

where a=4 σ/c is the radiation density constant.

If the temperature is split between ions and electrons, then the two temperature energy equations are given by:

$$\frac{\partial e_i}{\partial t} = -\frac{p_i}{\rho}\nabla\cdot u + \frac{\tau}{\rho}\nabla\cdot u - \nabla\cdot(k_i\nabla T_i) + Q_{ei} \quad (11)$$

and

$$\frac{\partial e_e}{\partial t} = -\frac{p_e}{\rho}\nabla\cdot u - \nabla\cdot(k_e\nabla T) - 4\sigma T_e^4\chi_{Planck} - Q_{ei} + \frac{\eta}{\rho}j^2 \quad (12)$$

where

$$Q_{ei} = \frac{3m_e Zk}{m_i^2}\frac{(T_e - T_i)}{\tau_e} \quad (13)$$

and the electron collision time is[25]

$$\tau_e = \frac{3}{4\sqrt{2\pi}}\frac{m_i\sqrt{m_e}}{Z\rho}\frac{(kT_e)^{3/2}}{\lambda}\frac{(4\pi\varepsilon_0)^2}{q^4}. \quad (14)$$

In SPFMax, several magnetic field solvers have been explored. This has been a challenging part during the development of this code. The challenge lies within the desire to have a model that handled self-consistently external circuits coupled to the computational domain as well as electric and magnetic field propagation across vacuum, dielectric and conductors. The basic approach [8] is that the plasma conducts current as a network of transmission lines integrating Kirchoff's voltage and current laws in which additional physics include back electromotive force (EMF), the Hall Effect and etc. as needed. Field propagation is accomplished by utilizing a superposition of current sources using Biot Savart's law. It was found that this brute force method was the simplest and least error prone way to enforce divergence of B equaling 0.

3 APPROACH

Simulations were conducted to explore different magnetic topologies resulting from variations in solenoidal windings. The three winding variations explored were ring shaped, bell shaped and a winding in the shape of the nozzle developed in the 1960s for nuclear thermal propulsion, The Nuclear Engine for Rocket Vehicle Application (NERVA). A major parameter explored in these simulations found a magnetic topology that provides a Lorentz force in the axial direction as the fusion plasma expands. A deuterium tritium plasma target was introduced inside each coil geometry and allowed to expand thermally with an initial density of 80 kg/m^3 and temperature of 1 keV. The target was 1 mm in radius, 1 cm in length and had a mass of 2.5 mg. The reason for the choice of density is due to the stopping power of the 4He, which gives a range comparable to the target radius at these densities. This is important for achieving a high fractional burnup in the target, which is assumed to produce an average thermal temperature of 1 keV in the fuel and propellant. It is clear that these assumptions as well as the feasibility of how to achieve these high densities in a DT plasma experiment will have to be explored much further beyond this initial study.

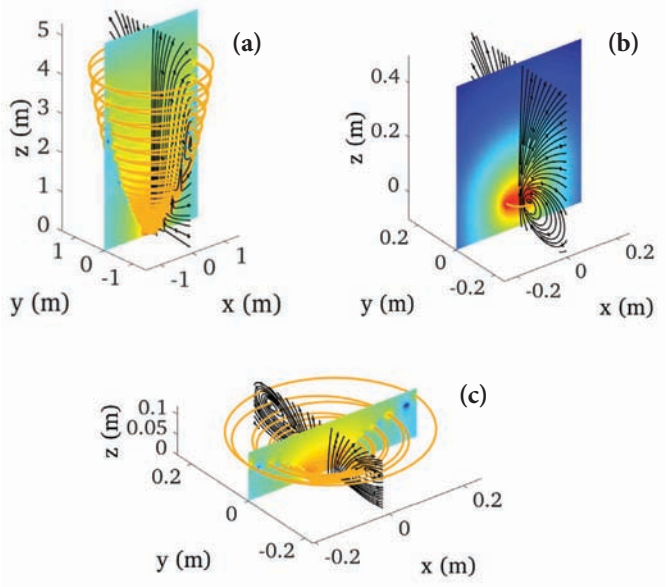

Fig.2 Magnetic nozzle shapes that were attempted but proved unsuccessful include (a) NERVA-shaped solenoid, (b) single-turn and (c) bell-shaped nozzles.

4 RESULTS

Figure 2 shows three of the initial coil geometries and magnetic field topologies attempted prior to arriving at a more successful design. The failed ideas are presented here in hopes that others can make them function or independently verify the potential of these designs. Since there has been no experimental or 3D simulation results on pulsed magnetic nozzles, the first attempt was a solenoidal field coil where the windings were in the shape of and to scale with the NERVA thermal rocket engine (Figure 2a). This shape was chosen because a starting point was needed and NERVA was an experimental program in advanced propulsion with hard data. Two types of simulations were attempted: one with the plasma born on a steady state field and one in which the coil was pulsed. In the former, an initial velocity of 20 km/s was applied; as a result, with pre-magnetization, the plasma was accelerated back towards the wrong end of the nozzle. This was similar to a refrigerator magnetic resisting the pull of removal from a ferromagnetic surface. In the pulsed configuration, a surface current was induced on the plasma inside the nozzle and some minor acceleration was observed; however, the primary force was in the radial direction. In such cases, ranges of current, pulse width and etc. were all tested and tried. It is important to note that the ratio of the magnetic field pressure to ram pressure during thermal expansion must exceed unity in order for the nozzle to work. Therefore, it was determined that a nozzle shape with a larger component of radial field was needed due to minimal acceleration observed in the NERVA-shape.

Figure 2b shows the second nozzle variation, a single turn ring, in which a larger component of radial field is visible from the stream lines. Nevertheless, there was no significant acceleration because the field lines in the radial direction are generally weak in comparison with the axial field inside the ring. In Figure 2c, a bell shape, like the bell of a trumpet, was devised to once again to increase the strength of the radial field; only a modicum of improvement was observed. In all three cases it was noted that the plasma experiences much stronger compression/confinement than expansion. The field strength under

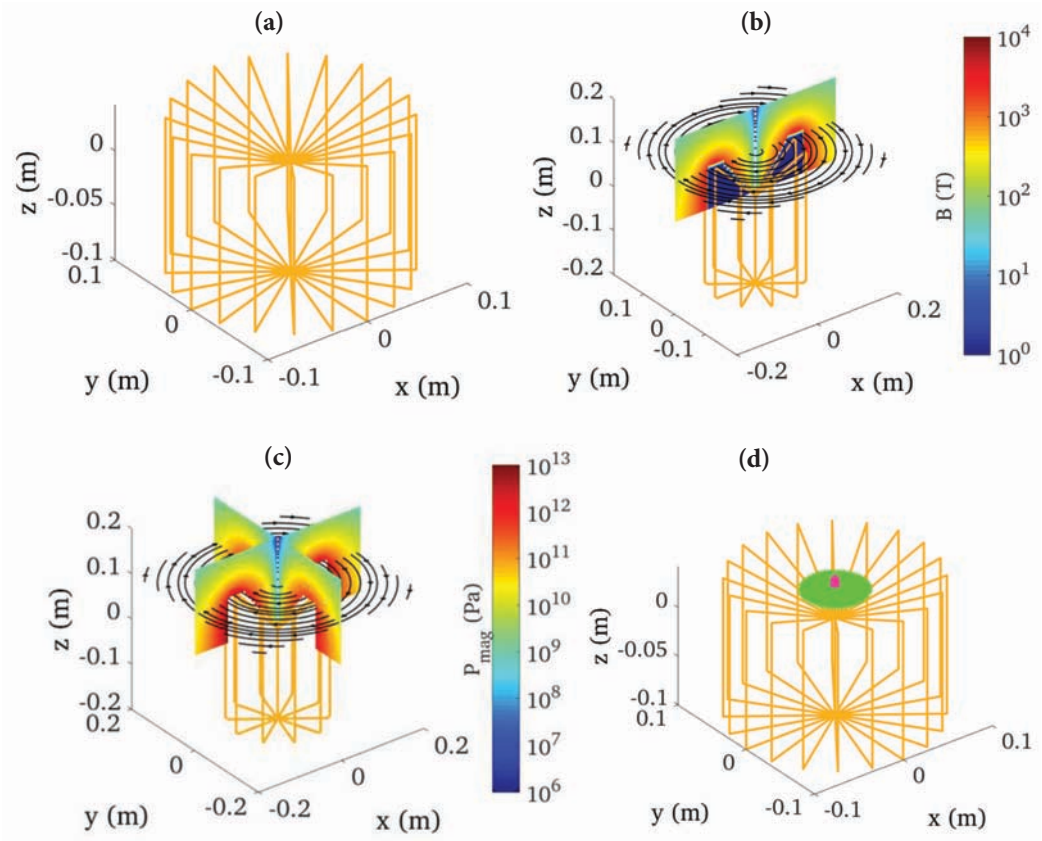

Fig.3 Magnetic nozzle shape that achieved a meaningful specific impulse, a) coil winding, b) magnetic field stream lines (nearly azimuthal) and contour flood plot of magnetic field strength, c) magnetic field pressure in [Pa] and d) nozzle with ablator plate (green) and initial target (magenta).

the coils was always stronger in the axial direction, so the $\boldsymbol{j}\times\boldsymbol{B}$ Lorentz force is pointed radially inward. To achieve a larger component in the axial direction, fundamental departure from the solenoid-family of nozzle shapes was taken.

It was hypothesized that it may be easier to generate strong azimuthal fields and rely on thermal expansion to induce radial currents; thus, increasing the force component in the axial direction needed for thrust (Fig. 3). The winding can be thought of as a central conductor through which current flows. Ultimately, near the plasma target, the current is split into a number of individual wires that flare in the shape of a nozzle with radial and axial components. At the nozzle exit, the wires are bent and return at some fixed radius. The wires will bend again to close the circuit back to the common center conductor. The winding in this geometry was subsequently recognized to resemble a deflection yoke, which was the technology used in cathode ray tubes in older televisions and analog oscilloscopes that directs the flow of electrons to a phosphor screen for displaying an image. In this winding, the magnetic field strength and direction are shown in Figure 3b. Noticeably, the field is almost 100% azimuthal in this geometry and the strength of the field is nearly 0 along the axis. The field strength grows rapidly in the direction of the field coils. The strength of the field in effect takes on the shape of a nozzle. In Figure 3c, the magnetic field pressure is shown with slices in the x=0 and y=0 planes; in one case, it is in plane with two opposing wires, while in the other plane, it is in between pairs of wires, thus indicating that the field pressure is fairly uniform. In Figure 3d, an ablator plate and initial target are shown to indicate the initial position of the plasma.

Figure 4 shows the initial position of the plasma and ablator plate to scale at t=0 and at 80 ns. The plasma expands at about 350 km/s, comparable to the initial sound speed. At 80 ns, the surface reaches the perimeter of the ablator plate. A few

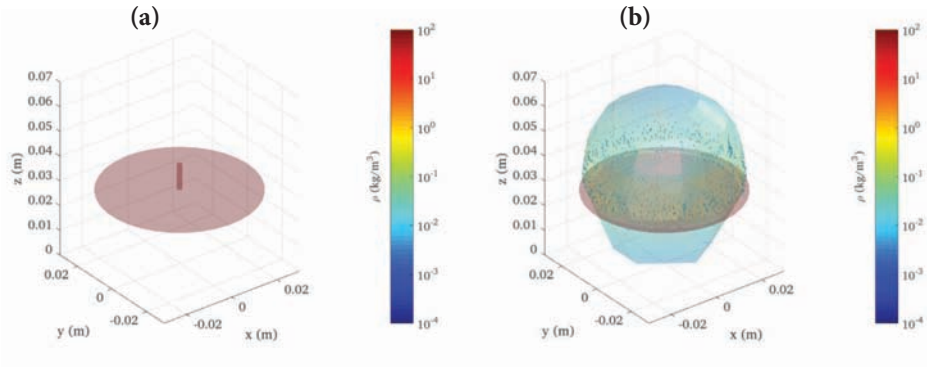

Fig.4 Expansion of cylindrical target with ablator plate shown for reference. In a), the target is shown to scale at t=0. In b), the time is 80 ns, the surface represents the boundary of the thermally expanded plasma, and vectors are visible indicating the production of current at the surface due to the back emf (expanding plasma against a steady field).

particles penetrate the plate, which was an error that was subsequently corrected by increasing the particle resolution in the plate. The radial expansion of the plasma moves into a rapidly changing magnetic field, which creates a motional back EMF that induces an image current in the plasma. This can be seen with the vectors that are mostly near the surface of the expanded plasma--in the direction antiparallel to the direction of the current in the coils. It should be noted that the case crashed at about 250 ns. Reasons for this are being explored and will be reported as this research matures.

The case that crashed was rerun without any field to try and isolate the ablator contribution to the thrust and specific impulse with that of the field. Figure 5 gives a time history of the axial (positive z-direction component) specific impulse for the target. The ablator plate with no field gives a peak 5000 seconds, while the magnetic nozzle reaches about 9000 seconds. This case is in no way optimized; however, the fact that the plasma remained stable and the magnetic nozzle provided marked improvement to the specific impulse achieved was encouraging.

With confidence in at least one path to a working magnetic nozzle, two interstellar-relevant deep-space missions were analyzed to determine the required propulsion performance. The first potential mission--made possible by a fusion propulsion system—was the deployment of a space telescope at a gravitational lensing point, beginning at a distance of 550 AU. Such a telescope would be capable of providing direct images of an extra-solar planet and thus would serve as a precursor for an interstellar mission. The second potential mission was the flyby of Alpha Centauri. To perform the calculations, a straight line trajectory analysis was performed using the 'Type II' performance equations developed and summarized by Moeckel [18]. Fig. 5 gives the mission performance for the parametric analysis in which trip time was varied. The payload was assumed to be 10 metric tons with a propulsion system specific power of 10 kW/kg.

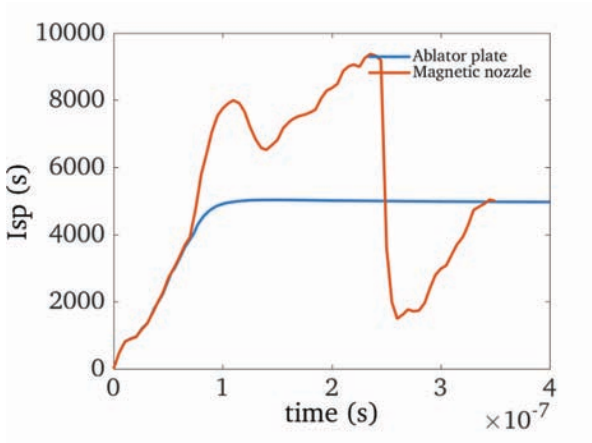

Fig.5 Comparison of ablator plate and magnetic nozzle specific impulse versus time.

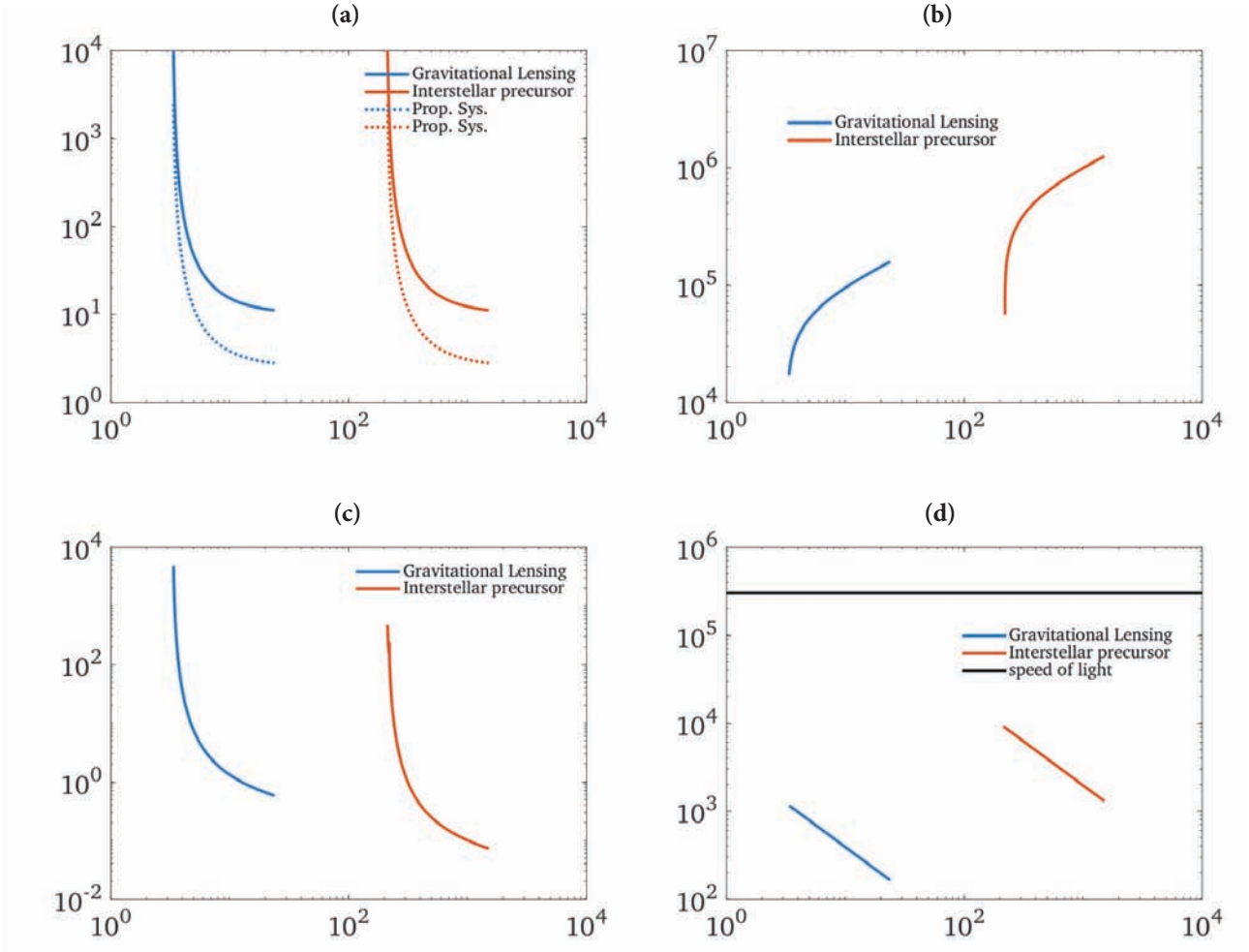

Fig.6 Parametric analysis for fusion propulsion flyby missions to a gravitational lensing focal point (550 AU) and Interstellar precursor (269,000 AU, the approximate distance to the Alpha Centauri system).

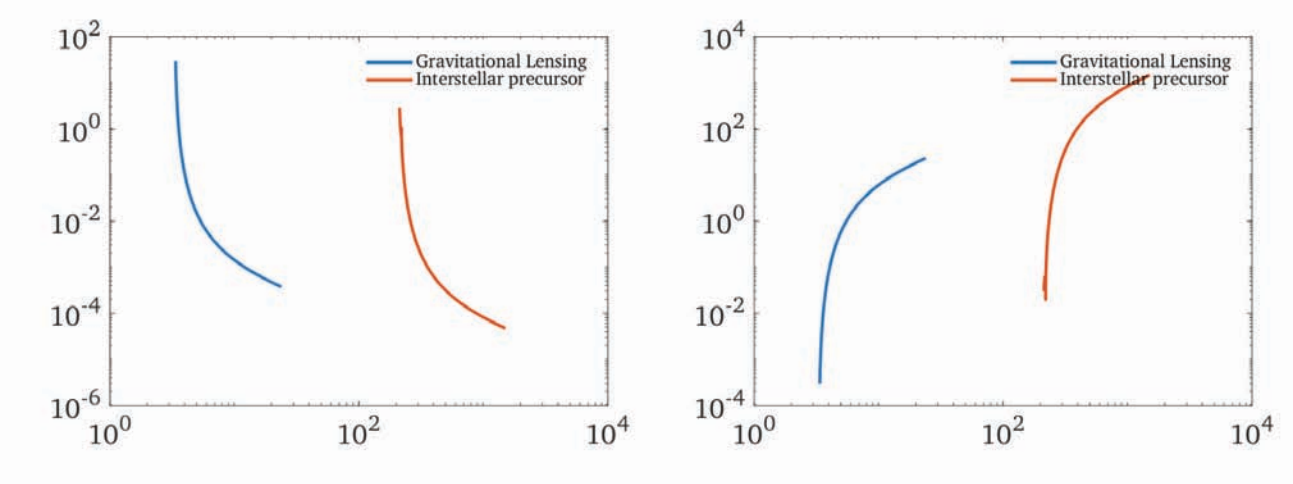

Fig.7 Propellant mass flow rate and pulse frequency required for a pulsed fusion propulsion system for the parametric mission analysis presented in Figure 6.

Additionally, the mass flow rate was derived from the thrust and specific impulse, and taking the initial target mass from the simulations, the required pulse frequency was determined, Figure 7. The mass flow rate is of the order of milligrams per second, and the required pulse frequency was of the order of 1 to 10 pulses per second, although results could vary at the very low and very high trip times in which mass is traded for mission trip time.

Of interest is the selection of a vehicle mass at the knee of the curve; thus, trading trip time for smaller vehicle masses. Table 1 provides the performance parameters needed to enable a mission to a gravitational lensing point as well as to Alpha Centauri. A vehicle mass of 15.3 metric tons was picked for the gravitational lensing missions, which gave a trip time of 10 years. The final burnout velocity was 392 km/s and requires a specific impulse of 94,000 seconds. For the interstellar flyby mission, the vehicle mass was selected at 1000 tons to bring down the lengthy trip time to 269 years. The specific impulse required for this choice of mass was 270,000 seconds, which approaches the upper limit achievable by thermal expansion of a fusion plasma. For both missions, the thrust is of the order of 1 N. Furthermore, the pulse frequency needed to achieve this varied from about three shots per second for the gravitational lensing mission to nine shots per second for the interstellar mission. Such pulse frequencies are readily achievable in existing pulse power systems, such as the capacitor bank at the Nike Laser Facility.

Comparable to Table 1, the specific impulse produced from the simulation is about a factor of 10 too low; however, the efficiency was about 20%. The route to the requisite specific impulse to make such deep-space missions achievable, with fusion or other pulsed systems, will be attainable with improved nozzle design, increased target temperature with due consideration to managing radiation loss and finite burn during expansion to maintain high pressures in the target in order to augment the rate of expansion.

5 CONCLUSIONS

3D simulations of a magnetic nozzle were performed using a SPH code coupled with SPFMax. Results suggest that magnetic nozzles are indeed capable of redirecting thrust from a plasma and found that coil shapes that create a mostly azimuthal magnetic field appear to produce a promising path toward efficient coil design. A specific impulse of 9000 s was achieved in such a nozzle with a cylindrical deuterium tritium plasma at 1 keV temperature, and the design was far from optimized. A null case was run without the field turned on, achieving only half of this specific impulse from the pusher plate, which was present in both cases. Mission analysis was performed to guide the needed improvements in the overall design, coupling fusion to magnetic nozzle performance. A specific impulse of 94,000 seconds is required for a 10 year flyby of a 550 AU gravitational lensing mission, while 270,000 s Isp is needed for a 269 year flyby of Alpha Centauri. Future work will include refinements to the coil design and burn physics during the thermal expansion to increase the efficiency and energy added to the plasma. It appears that these high specific impulse requirements are possible to enable such missions.

Acknowledgments

This work was supported in part by NASA contract NNM11AA01A.

TABLE 1 Input parameters of the simulation

Destination	Trip time (years)	Isp (s)	IMLEO (metric tons)	Thrust (N)	Shot frequency (1/s)	Mass flow rate (mg/s)	ΔV (km/s)
Gravitational Lensing	10	$9.4x10^4$	15.3	0.66	2.9	0.72	392
Alpha Centauri	269	$2.7x10^5$	1000	1.39	8.8	0.48	7,280

REFERENCES

1. J. Cassibry, R. Cortez, M. Stanic, A. Watts, W. Seidler, R. Adams, G. Statham and L. Fabisinski, "Case and Development Path for Fusion Propulsion," J*ournal of Spacecraft and Rockets*, vol. 52, no. 2, pp. 595-611, 2015.
2. J. Miernik, G. Statham, L. Fabisinski, C. Maples, R. Adams, T. Polsgrove, S. Fincher, J. Cassibry, R. Cortez, M. Turner and T. Percy, "Z-Pinch fusion-based nuclear propulsion," *Acta Astronautica*, vol. 82, pp. 173-182, 2013.
3. R. Adams, R. Alexander, J. Chapman, J. Fincher, S. Philips, A. Polsgrove, T. Wayne, B. Patton, G. Statham, S. White and Y. Thio, "Conceptual Design of In-Space Vehicles for Human Exploration of the Outer Planets," NASA Technical Rept. 2003-212691, 2003.
4. N. Schulze, "Fusion Energy for Space Missions in the 21st Century," NASA Office of Safety and Mission Quality, NASA Technical Memorandum TM4298.
5. "Nuclear Pulse Space Vehicle Study," George C. Marshall Space Flight Center, Huntsville, AL, 1964.
6. K. Schillo, *Three-Dimesional Modeling of an Ideal Nozzle for Addvanced Propulsion, a thesis,* Huntsville, AL: University of Alabama in Huntsville, May 2014.
7. G. Romanelli, A. Mignone and A. Cervone, "Pulsed fusion space propulsion: Computational Magneto-Hydro Dynamics of a multi-coil parabolic reaction chamber," *Acta Astronautica*, vol. 139, no. October, pp. 528-544, 2017.
8. J. Cassibry, R. Cortez, C. Cody, S. Thompson and L. Jackson, "Three Dimensional Modeling of Pulsed Fusion for Propulsion and Terrestrial Power Using Smooth Particle Fluid with Maxwell Equation Solver (SPFMaX)," in 53rd *AIAA/SAE/ASEE Joint Propulsion Conference*, Atlanta, GA, 2017.
9. J. J. Monaghan, "Smoothed Particle Hydrodynamics," *Reports on Progress in Physics*, vol. 68, pp. 1703-1759, 2005.
10. J. P. Morris, J. F. Patrick and Y. Zhu, "Modeling Low Reynolds Number Incompressible Flows Using SPH," *Journal of Computational Physics*, vol. 136, pp. 214-226, 1997.
11. J. H. VanSant, "Conduction Heat Transfer Solutions," UCRL-52863-Rev. 1, Lawrence Livermore National Laboratory, CA, 1983.
12. R. Fatehi and M. T. Manzari, "Error estimation in smoothed particle hydrodynamics and a new scheme for second derivatives," *Computers and Mathematics with Applications*, vol. 61, no. 2, pp. 482-498, 2011.
13. M. A. Rodriguez and J. T. Cassibry, "A 3-D Smoothed-Particle Hydrodynamics Model of Electrode Erosion," *IEEE Transactions on Plasma Science*, vol. 45, no. 11, pp. 3030-3037, 2017.
14. J. Bonet and T. S. L. Lok, "Variational and momentum preservation aspects of Smooth Particle Hydrodynamics Formulations," *Computer Methods in Applied Mechanics and Engineering*, vol. 180, pp. 97-115, 1996.
15. S. J. Watkins, A. S. Bhattal, N. Francis, J. A. Turner and A. P. Whitworth, "A new prescription for viscosity in Smoothed Particle Hydrodynamics," A*stronomy and Astrophysics*, vol. 119, pp. 177-187, 1996.
16. J. H. Jeong, M. S. Jhon, J. S. Halow and J. v. Osdol, "Smoothed particle hydrodynamics: Applications to heat conduction," *Computer Physics Communications*, vol. 153, no. 1, pp. 71-84, 2003.
17. Y. B. Zel'dovich and Y. P. Raizer, *Physics of Shock Waves and High-Temperature Hydrodynamic Phenomena*, Meneola, New York: Dover Publications, Inc., 2000.
18. W. E. Moeckel, "Comparison of Advanced Propulsion Concepts for Deep Space Exploration," *Journal of Spacecraft and Rockets*, vol. 9, no. 12, pp. 863-868, 1972.
19. G. Liu and M. Liu, Smoothed Particle Hydrodynamics: A Meshfree Particle Method, 2003.
20. J. J. MacFarlane, I. E. Golovkin and P. R. Woodruff, "HELIOS-CR – A 1-D radiation-magnetohydrodynamics code with inline atomic kinetics modeling," *Journal of Quantitative Spectroscopy and Radiative Transfer*, vol. 99, no. 1-3, pp. 381-397, 2006.
21. J. Monaghan, "Smoothed particle hydrodynamics," *Reports on Progress in Physics*, vol. 68, pp. 1703-1759, 2005.
22. I. Lindemuth and R. Siemon, "The fundamental parameter space of controlled thermonuclear fusion," *American Journal of Physics*, vol. 77, no. 5, pp. 407-416, 2009.
23. I. R. Lindemuth and R. C. Kirkpatrick, *Nuclear Fusion*, vol. 23, p. 263, 1983.
24. A. M. Buyki and et al, "Investigations of Thermonuclear Magnetized Plasma Generation in the Magnetic Implosion System MAGO," All-Russion Institute of Experimental Physics, Arzamas-16, Nizhny Novgorod Region, Russia.
25. J. T. Cassibry, M. A. Rodriguez and K. J. Schillo, "Test Suite for Hydrodynamic Modeling for Plasma Driven Magneto-Inertial Fusion," in 52nd *Annual AIAA/SAE/ASEE Joint Propulsion Conference*, Salt Lake City, UT, July 2016.

Received 15 May 2018 **Approved** 25 September 2018